energies

MDPI

Article

Optimal Design of a Multibrid Permanent Magnet Generator for a Tidal Stream Turbine

Khalil Touimi [1,2], Mohamed Benbouzid [1,3,*] and Zhe Chen [4]

1 Institut de recherche Dupuy de Lôme (UMR CNRS 6017 IRDL), University of Brest, 29238 Brest, France; Khalil.Touimi@univ-brest.fr
2 École Militaire Polytechnique, 16111 Alger, Algeria
3 Logistics Engineering College, Shanghai Maritime University, Shanghai 201306, China
4 Department of Energy Technology, Aalborg University, 9220 Aalborg, Denmark; zch@et.aau.dk
* Correspondence: Mohamed.Benbouzid@univ-brest.fr; Tel.: +33-2980-18007

Received: 15 November 2019; Accepted: 16 January 2020; Published: 19 January 2020

Abstract: Tidal stream energy is acquiring more attention as a future potential renewable energy source. Considering the harsh submarine environment, the main challenges that face the tidal stream turbine (TST) industry are cost and reliability. Hence, simple and reliable technologies, especially considering the drivetrain, are preferred. The multibrid drivetrain configuration with only a single stage gearbox is one of the promising concepts for TST systems. In this context, this paper proposes the design optimization of a multibrid permanent magnet generator (PMG), the design of a planetary gearbox, and afterwards analyzes the multibrid concept cost-effectiveness for TST applications. Firstly, the system analytical model, which consists of a single-stage gearbox and a medium speed PMG, is presented. The optimization methodology is afterwards highlighted. Lastly, the multibrid system optimization results for different gear ratios including the direct-drive topology are discussed and compared where the suitable gear ratio (topology) is investigated. The achieved results show that the multibrid concept in TST applications seems more attractive than the direct-drive one especially for high power ratings.

Keywords: tidal stream turbine; multibrid concept; direct-drive; permanent magnet generator; single stage gearbox; design optimization

1. Introduction

Tidal stream energy is one of the promising renewable energy sources, which is highly predictable and its potential can exceed 120 GW [1,2]. It is mainly harnessed by horizontal axis turbines where the marine current kinetic power is converted into an electrical one. Despite the infancy of tidal stream turbine (TST) technologies, various machines and prototypes have been developed in recent decades, and different concepts are competing for supremacy [3–5]. In addition to the technology infancy, the harsh submarine environment increases the criticality of the TST subsystems. Therefore, the main challenges that face the tidal stream turbine industry are the energy cost and the system reliability, which means simple and reliable technologies should be adopted. Drivetrain and generator topology choice typically affects the availability of the system as well as the produced energy cost. The main TST configuration types are gearless TST (direct-drive), mechanically geared TST, and magnetically geared TST [6–8].

Direct-drive topology (Figure 1), which was designed to avoid gearbox failures in wind turbines, is attractive due to its simplicity and its high reliability. However, direct-drive generators are non-standard electric machines and have some disadvantages such as the heavy weight, large diameter, and therefore high cost. Geared generators are compact, robust, and economically available compared

to direct-drive ones, in addition to the fact that mechanical gearbox technologies are mature. Moreover, authors in [9] addressed the criticality of wind turbine subsystems in different sites and provided a comparison between geared and direct-drive wind turbines. The study shows that direct-drive systems are less reliable than geared ones. However, mechanical gearboxes are still critical subsystems, which can lower tidal stream turbines availability [10]. In [11] a comparative study between direct-drive tidal stream turbines and gearbox driven ones has been carried out, where the result suggested the multibrid concept as an alternative compact drivetrain for TST applications in terms of reliability and availability.

Figure 1. OpenHydro/Naval Energies direct-drive tidal stream turbine [4].

The multibrid configuration (Figure 2a), with a single-stage planetary gearbox associated to a medium speed PMG, combines the advantages of both geared and gearless drivetrain [12]. Indeed, a medium speed generator is cheaper and more efficient than a direct-drive one and a single-stage gearbox is lighter and more reliable than a multiple-stage one. Wind turbines manufacturers have developed multibrid technology such as Multibrid (M5000) and WinWind (WWD-3) [13] (Figure 2b), [14]. The same concept has been designed, realized, and tested for a small scale TST system in the Chinese Zhoushan water channel [15] (Figure 3).

(**a**) (**b**)

Figure 2. The multibrid concept: (**a**) Schematic illustration [12], (**b**) The AREVA Multibrid M5000 5 MW wind turbine nacelle [11].

The cost of a Multibrid TST depends on the gearbox ratio and the generator diameter. Gearboxes with high gear ratio are heavier and more expensive. However, their high-speed output leads to cheaper generators with low diameter. Hence, to determine the appropriate gearbox ratio and generator dimensions for given specifications, a system optimization is required by minimizing its active parts cost.

Figure 3. Small scale multibrid tidal stream turbine [15].

Previous studies on wind turbine systems compared geared generators (including single stage gearbox driven ones) to direct-drive generators in terms of cost. In [16], the authors compared quantitatively different drive-train configurations and different generator topologies. In this study, which highlights the multibrid concept, the design of the generators is not optimized and the gear ratio is chosen in advance. In [17] and based on [16], the authors have estimated and compared the cost of energy of different drive-train configurations. Unlike the above-cited papers, Hui et al. [12] have investigated gearbox ratios and power ratings cost-effective ranges of multibrid permanent magnet wind generators including direct-drive ones. Concerning TST design optimization, in [5,18], the authors compared different optimized direct-drive PMG topologies (rim-driven vs. pod assembly and radial flux vs. axial flux PMG). However, for the geared drive-train configuration especially, the multibrid concept was not considered. Even if the wind turbine systems seem similar to TST ones, some fundamental differences on design and operation require more investigation, such as biofouling and marine current turbulence [19,20]. Therefore, both the blades and yaw pitch subsystems are avoided due to their high criticality in such a hostile environment [9].

In this paper, a design optimization of PMG for TST system is proposed in order to analyze the cost-effectiveness of the multibrid concept and compare it to the direct-drive one. In this context, the Multibrid TST analytical model is presented and it consists of: the turbine model, the single stage planetary gearbox model, the three-phase PMG two-dimensional (2D) electromagnetic model, and the power electronics converter model. Figure 4 is therefore illustrating a grid-connected single stage gearbox driven PMG, highlighting each subsystem. The proposed design optimization process is performed using the interior-point method to minimize the active material cost of the generator. The suitable drivetrain configuration is afterwards investigated for different power ratings (500 kW, 1.5 MW, and 5 MW) and the achieved results are compared and discussed.

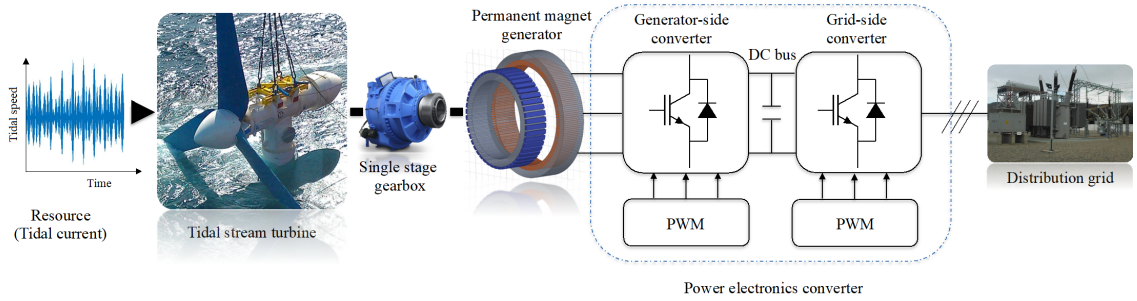

Figure 4. Scheme of a grid-connected single stage permanent magnet generator-based tidal stream turbine.

2. System Modeling

2.1. Renewable Resource and Tidal Turbine Modeling

Tidal current velocity data in the site near Ouessant Island were collected by the French navy hydrographic and oceanographic service [21]. The amplitude and direction measurements of the tidal current velocity are done hourly during one year (8760 h). The optimal direction, which provides the maximum of energy, is calculated as described in [22] (Figure 5). Tidal speed through the optimal direction is shown in Figure 6.

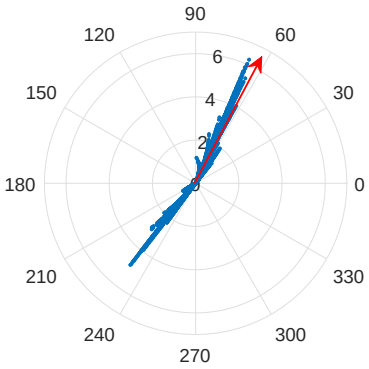

Figure 5. Tidal velocity in polar coordinates.

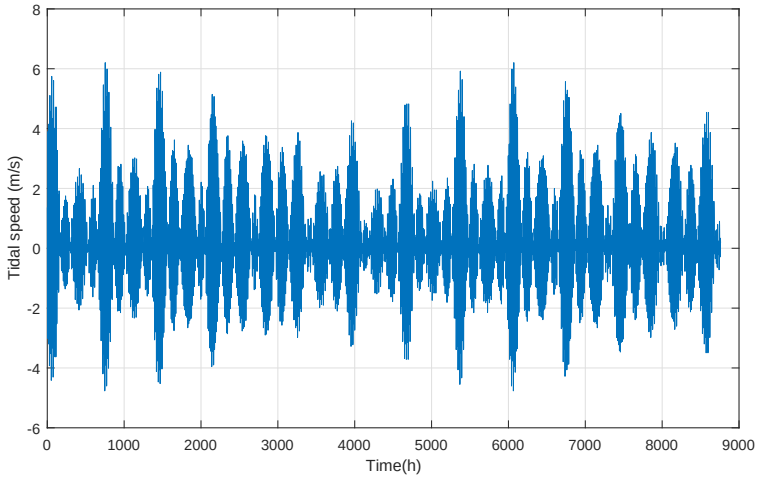

Figure 6. Tidal velocity in the Ouessant Island.

2.1.1. Power and Energy Calculation

Energy calculation is done considering the optimal angle direction (61°). Concerning the input shaft power from a tidal turbine, it is calculated as a function of tidal currents speed and the turbine rotor diameter.

$$P_T = \frac{1}{2}\rho C_p(\lambda,\beta)A_t v^3, \tag{1}$$

where $A_t = \frac{1}{4}\pi D^2$ is the turbine blade swept area, ρ is the sea water density, $C_p(\lambda,\beta)$ is the power coefficient which is a function of tip speed ratio (λ) and the pitch angle of the tidal turbine blades (β).

The annual energy production (AEP) can be calculated by summing the harnessed energy in each hour (the tidal current speed is assumed non-variable). Figure 7 shows the energy distribution according to tidal current speed amplitude in the Ouessant site.

$$AEP = \int_{v_i}^{v_n} P_T(|v|)OCC(|v|)dv + P_{Tr}\int_{v_n}^{v_c} OCC(|v|)dv, \tag{2}$$

where v_i is the cut-in tidal current speed, v_c is the cut-out tidal current speed, v_n is the rated tidal current speed, and P_{Tr} is the rated input shaft power.

The $OCC(|v|)$ function represents the tidal current speed amplitude distribution (Figure 8).

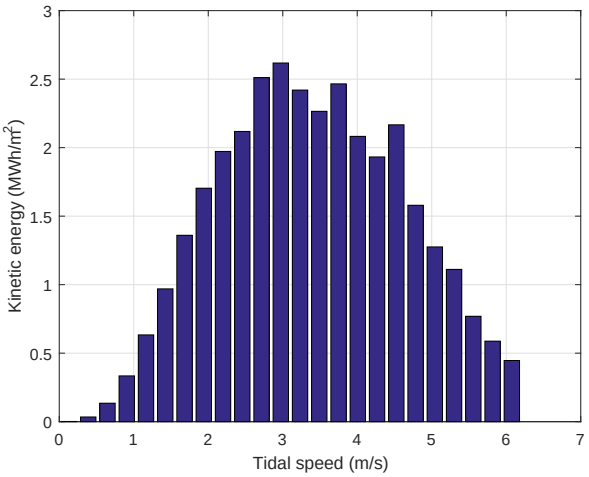

Figure 7. Tidal current energy distribution.

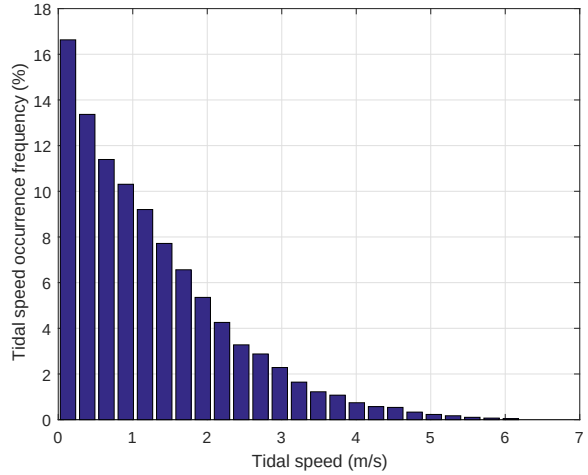

Figure 8. Tidal current amplitude speed distribution.

2.1.2. Power Rating Choice

To harness all the energy, a maximal power should be chosen as a rated one and an oversized system will be required. In wind turbines, mechanical limitation of power using blade or yaw pitch subsystems are adopted. However, due to the harsh submarine conditions such mechanical subsystems should be avoided. An alternative using an over-speed power limitation is adopted in this study. In this context, when the input power is less than the rated one, the power coefficient is maintained at his maximum ($C_{pmax} = 0.455$) (Table 1). However, when the input power is higher than the rated one, the generator accelerates and reduces the power coefficient. This methodology is detailed in [8]. The power rating (limitation power) is chosen around 30% of the maximum power where 90% of the total energy can be harnessed (Figure 9). As the swept area considered is 1 m^2, the same power ratio of 30% is maintained, and for each power rating (500 kW, 1.5 MW, 5 MW) only the blade's diameter (swept area) is calculated.

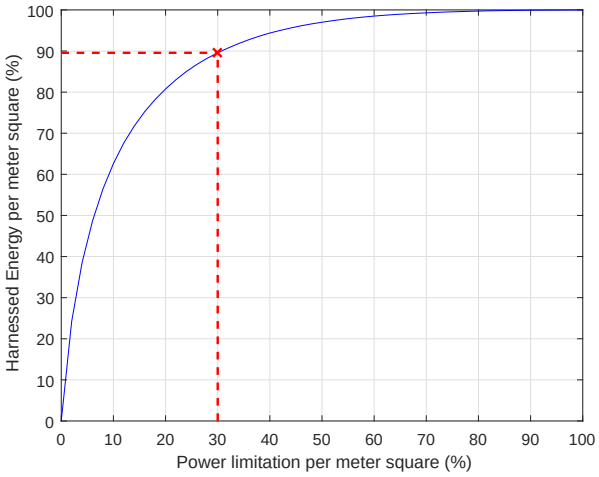

Figure 9. Harnessed energy rate versus power limitation rate.

2.2. Gearbox Modeling

The gearbox converts the turbine rotor slow rotational speed and high shaft torque to high rotational speed and low torque. The more its gear ratio is high, the more its cost and weight increases. However, the opposite happens to the generator because its input shaft torque decreases. It exists two main types of gear trains: parallel shaft and planetary. In this study, a planetary single stage gearbox is considered due to its high power density (Figure 10). The volume of each part of the planetary gearbox is estimated to calculate its total mass [23,24].

$$\sum FWd^2 = FWd_s^2 + FWd_p^2 + K_r FWd_r^2, \tag{3}$$

where FW is the face width of the gear, d_s, d_p, and d_r are the diameter of the sun, the planets, and the ring gear respectively. FWd^2 presents the gear volume and $K_r = 0.4$ is a scaling factor and it is selected from [23,24].

The weight of the planetary single stage gearbox is a function of the gear ratio and the transmitted shaft torque [25]. Equation (4) is developed to obtain the planetary gearbox total weight.

$$G_{gear} = \frac{W_c}{36050} \frac{2(10^3) T_m K_{ag}}{K_f} \left[\frac{1}{Z} + \frac{1}{Z r_{sn}} + r_{sn} + r_{sn}^2 + K_r \frac{(1 + (r_{sn})^{-1})}{Z} (r_{ratio} - 1)^2 \right] \tag{4}$$

In the last Equation (4), T_m is the gearbox output shaft torque and K_{ag} is the application factor. It is chosen from [23] among different application factors. In fact, a factor of 1.0 is chosen when we have a perfectly smooth turbine driving a perfectly smooth generator always at a constant speed (no frictions and no vibrations). Because of the high torque fluctuations due to the high marine energy density [26], an application factor of 1.5 is chosen. K_f is an index of tooth loads intensity and it is empirically estimated from [23]. W_c, which is the weight constant, is also estimated from [23]. r_{ratio} is the single stage gearbox ratio (between the carrier and the sun gear), $r_{sn} = (r_{ratio}/2) - 1$ is the ratio between the sun and planet gears, and Z is the number of planet gears (Table 1).

The estimated cost of the single stage gearbox is given as

$$C_{gear} = c_{gear} G_{gear}, \tag{5}$$

where c_{gear} is the specific cost of the single stage gearbox (Table 1).

Concerning losses, only speed dependent ones are considered (seal losses and lubricant losses). Regarding power-dependent losses, they are negligible compared to speed dependent ones [27].

$$p_{gear} = k_g P_N \frac{n_r}{n_{r_N}} \tag{6}$$

In the precedent Equation (6), k_g is the speed-dependent losses constant, P_N is the rated power of the TST, n_r is the rotor speed, and n_{r_N} is the rated rotor speed.

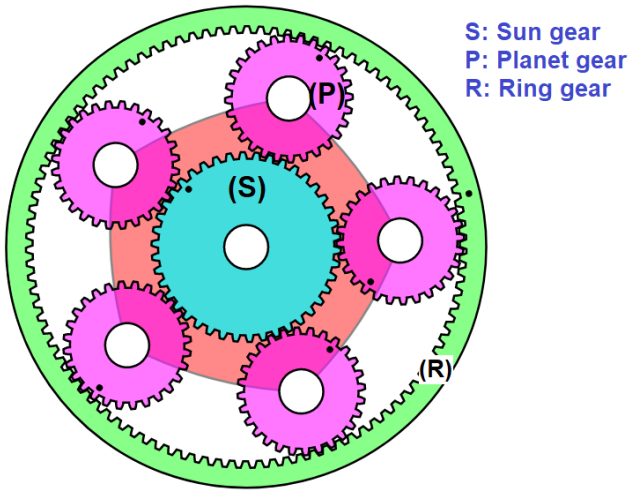

Figure 10. Illustration of a planetary gearbox with five planet gears.

2.3. Single Stage Geared PMG Design

The generator considered in this paper is a three phase radial flux permanent magnet one [8]. Figure 11 shows the geometric parameters of one pair of poles and its structure. The magnets are surface mounted and the generator curvature is assumed insignificant. For design purposes, the adopted modeling is a 2D analytical electromagnetic model based on magnetic circuit calculation [18,28]. The objective is to calculate the size of the generator knowing its specifications.

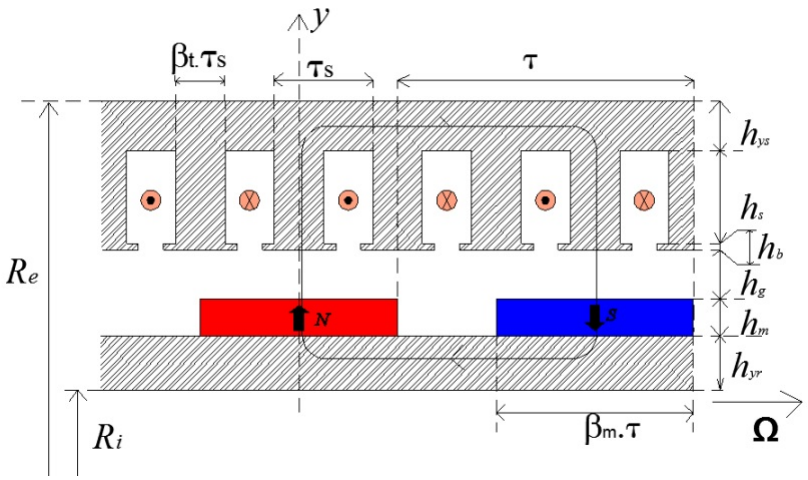

Figure 11. Basic dimensions of one pair of poles [8].

2.3.1. Electromagnetic Torque

The average electromagnetic torque results from the interaction between the fundamental electromotive forces and the currents of the phases (considered sinusoidal) at the nominal operating point [29].

$$< T_{EM} >= 4\sqrt{2} A_L k_{b1} B_{g_{max}} R_s^2 L_m \xi_{3D} \sin(\beta_m \frac{\pi}{2}) |\cos(\psi)|, \tag{7}$$

where A_L is the current loading in the stator, $B_{g_{max}}$ is the maximum air-gap flux density under the magnet, k_{b1} is the first harmonic winding factor, ψ is the phase shift between the fundamental of the electromotive force and the current, R_s is the stator radius, L_m is the equivalent core length, and ξ_{3D} is a corrective coefficient which takes into consideration the 3D flow leakage.

2.3.2. Air-Gap

The mechanical air-gap is given by the following empirical formula [30]

$$h_g = 2k_D R_s, \tag{8}$$

where k_D is a coefficient, which considers the deformations caused by the forces acting on the rotating rotor.

The additional Carter air-gap $h_{g'}$ is calculated as [30]

$$h_{g'} = (k_c - 1)(h_g + \frac{h_m}{\mu_{rm}}), \tag{9}$$

where k_c is the Carter factor, h_m is the magnet height, and μ_{rm} is the magnets relative permeability.

2.3.3. Magnet Height

The magnet height model calculation considers inter-polar 2D leakage flow [28]

$$h_m = \frac{\tau}{2\pi}\left[\ln\left(\frac{(\mu_{rm}+1)B_{g_{max}}\exp\frac{-\pi}{\tau}(h_g+h_{g'}) - \frac{(\mu_{rm}-1)}{(\mu_{rm}+1)}\exp\frac{\pi}{\tau}(h_g+h_{g'}) - 2B_r}{(\mu_{rm}+1)B_{g_{max}}\exp\frac{\pi}{\tau}(h_g+h_{g'}) - \frac{(\mu_{rm}-1)}{(\mu_{rm}+1)}\exp\frac{-\pi}{\tau}(h_g+h_{g'}) - 2B_r}\right)\right], \tag{10}$$

where B_r is the magnet's remanent flux density and $B_{g_{max}}$ is the maximum air-gap flow density, and τ is the pole pitch.

2.3.4. Slot Height

The slot height depends on the current loading A_L, the fill factor k_f, and the teeth pitch ratio β_t.

$$h_s = \frac{A_L}{k_f J(1-\beta_t)} \tag{11}$$

2.3.5. Stator and Rotor Yoke Height

The stator yoke height h_{ys} is determined in a way to avoid its saturation. With the same principle, the rotor yoke height h_{yr} is developed [28].

$$h_{ys} = \beta_m \frac{\pi R_s}{2p}\frac{B_{g_{max}}}{B_{sat}} + \frac{1}{3}\frac{\mu_0\mu_{rm}\sqrt{2}A_L\pi^2R_s^2}{(h_m+\mu_{rm}(h_g+h_{g'}))S_{pp}mp^2B_{sat}}, \tag{12}$$

$$h_{yr} \approx h_{ys} \tag{13}$$

where S_{pp} is the number of slots per pole per phase, m is the phases number, and p is pole pairs number.

2.3.6. Teeth Pitch Ratio

The teeth pitch ratio β_t is calculated in a way to assure a non saturation of the generator when it is over-fluxed ($\psi = \pi/2$) and the air-gap flow density is at its maximum $Bg = Bg_{max}$ along the pole [28].

$$\beta_t = \frac{B_{g_{max}}}{B_{sat}} + \frac{\mu_0\mu_{rm}\sqrt{2}A_L\pi R_s}{(h_m+\mu_{rm}(h_g+h_{g'}))S_{pp}mpB_{sat}} \tag{14}$$

2.3.7. Maximum Magnetic Field

To avoid the irreversible permanent magnet demagnetization, the maximum magnetic field H_{max} has to be less than the PM coercive magnetic field H_{cj}. The maximum magnetic field is calculated in the worst scenario where stator flow density is opposite to the rotor flow density. H_{max} will be introduced as a constraint in the optimization process [28].

$$|H_{max}| = \frac{\sqrt{2}A_L \pi R_s}{(h_m + \mu_{rm}(h_g + h_{g'}))S_{pp}mp} + \frac{(h_g + h_{g'})B_{g_{max}}}{\mu_0 h_m} \tag{15}$$

2.3.8. Iron Losses

The specific iron losses are estimated by using the Steinmetz formula [31,32]

$$p_{Fe} = 2p_{Fe0h}(\frac{f_e}{f_0})(\frac{\widehat{B}_{Fe}}{\widehat{B}_0})^2 + 2p_{Fe0e}(\frac{f_e}{f_0})^2(\frac{\widehat{B}_{Fe}}{\widehat{B}_0})^2, \tag{16}$$

where f_e is the field frequency in the iron, p_{Fe0h} represents the specific hysteresis loss, p_{Fe0e} represents the specific eddy current loss in the laminated stator core for a frequency f_0 of 50 Hz and a flux density $\widehat{B_0}$ of 1.5 T.

2.3.9. Synchronous Inductance

The synchronous inductance L_s is the sum of the magnetizing inductance L_{sm} and the leakage inductance L_{sl}. It is calculated as [30]

$$L_{sm} = \frac{6\mu_0 L_e R_s (k_w N_s)^2}{\pi p^2 (h_g + h_{g'})}, \tag{17}$$

where μ_0 is the vacuum permeability constant and N_s is the number of turns of the phase winding.

Only slot leakage and the end-winding leakage inductances are considered to calculate the leakage inductance L_{sl}. Skew leakage inductance is ignored because the stator slots are not skewed.

2.4. Power Electronic Converter Design

A two level back-to-back pulse width modulation (PWM) full scale converter is used to inject power from the generator to the grid. Its specific cost estimate is presented in Table 1. Concerning losses rate, they are considered to be about 3% at the rated load [33].

Table 1. Modeling parameters of the tidal stream turbine system.

Tidal Stream Turbine			
Rated power P_N [MW]	0.5	1.5	5
Rated rotor speed n_{r_N} [rpm]	80.3	47.0	25.8
Rotor diameter D [m]	6	10.3	18.8
Cut it tidal current speed v_i [m/s]		1.0	
Cut out tidal current speed v_{out} [m/s]		6.2	
Maximum power coefficient C_{pmax}		0.455	
Optimum tip speed ratio λ_{opt}		5.90	
Sea water density [kg/m^3]		995.6	

Table 1. *Cont.*

Single Stage Planetary Gearbox	
Gearbox application factor K_{ag}	1.5
K-factor K_f [N/mm^2]	2.76
Gearbox weight constant W_c	0.6
Planet gears number Z	6
Gearbox specific cost c_{gear} [€/kg]	6
Speed dependent losses constant k_g [%]	1.5
PMG System	
Hysteresis losses at 1.5 T and 50 Hz p_{Fe0h} [W/kg]	2
Eddy-current losses at 1.5 T and 50 Hz p_{Fe0e} [W/kg]	0.5
Specific cost of electrical steel c_{Fe} [€/mT]	449.77
Specific cost of copper c_{Cu} [€/mT]	4259.18
Specific cost of NdFeB magnet c_m [€/mT]	84,538.60
Specific cost of power electronics c_{conv} [€/kW]	40

3. Design Optimization

The design optimization is based on the modeling of each part of the system (the turbine, the gearbox, the power electronics converters, and the PMG generator). The electromagnetic specifications are all the fixed design parameters, the gearbox ratio is chosen before the optimization process starting, and tidal power specifications are calculated from tidal current speed data. The analytical model can be represented by a non-linear function, which has as input a geometrical design variables vector. To evaluate the cost-function, an iterative inversion of the non-linear model is adopted. By considering the constraint, the interior-point optimization technique is used to minimize the cost-function. The optimal design is the one which has the lowest cost (Figure 12).

3.1. Cost-Function

The TST cost depends on its active materials weight, its structure cost, and its manufacturing cost. In this study, only the generator's active materials cost is considered in addition to the gearbox and the power electronic converter costs. The active material cost depends on the size of each material. Hence, the generator cost is calculated only from the size parameters $G = (L_m, hs, hm, hys, \beta_t)$.

$$C_g = c_{Cu}G_{Cu} + c_{Fe}G_{Fe} + c_mG_m \tag{18}$$

$$C_{TST} = C_g + C_{gear} + C_{conv}, \tag{19}$$

where C_{gear} is the single stage gearbox cost, C_{conv} is the estimated power electronics cost, c_{Cu}, c_{Fe}, c_m are the copper, the iron, and the permanent magnet specific costs, and G_{Cu}, G_{Fe}, G_m are the copper, the iron, and the permanent magnet weights, respectively.

The cost-function depends on the gearbox ratio and the size parameters of the PMG. However, if the analytical modeling is considered, the PMG cost will depend only on the following variables $X = (A_L, J, B_{g_{max}}, p, R_s)$.

$$X^* = min_{X\in\mathbb{D}}||C_g(X)||, \tag{20}$$

where X is the vector including the independent variables $(A_L, J, B_{g_{max}}, p, R_s)$ and $\mathbb{D}$ is the set of possible solutions.

3.2. Optimization Constraints

The optimization is performed under electromagnetic and mechanical constraints, which define the $\mathbb{D}$ set.

The first constraint on the pole pair number is related to the maximum electrical frequency. In fact, a high pole pair number leads to a higher electrical frequency resulting in high iron losses. To avoid this, the maximum electrical frequency (f_{max}) allowed in laminated steel core is limited, which can be considered as a limitation of the pole pair number. The second constraint is related to the ratio of slot depth to slot width. This ratio must be in the range of 4–10 to avoid excessive mechanical vibrations [12,34]. This limitation is converted to two additional constraints on the pole pair number.

The maximum magnetic field $H_{max}(X)$ (see Equation (15)) is limited to be smaller than the permanent magnet coercive field to prevent demagnetization. The current density J and the loading current A are limited in the range of 3–6 A/mm^2 and 40–60 kA/m respectively [12]. The generator efficiency is considered to be greater than 0.96. On the other hand, the phase voltage root mean square is fixed to 690 V.

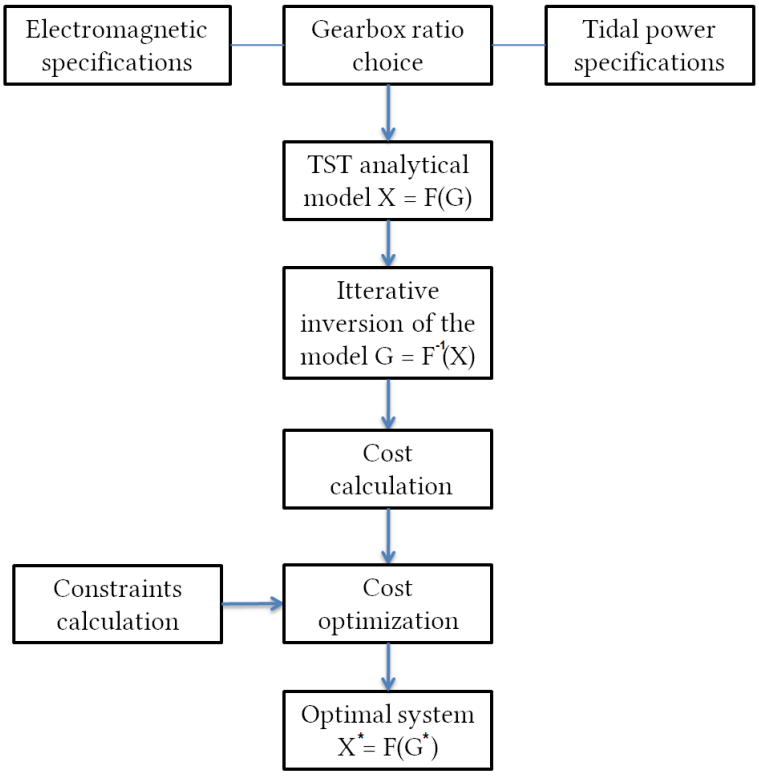

Figure 12. Flowchart describing the design optimization procedure.

4. Design Results and Discussion

To investigate the cost-effectiveness of the multibrid concept in TST systems, design optimization of the system is performed for different gearbox ratios (1:1,3:1,5:1,7:1,9:1,11:1) and different power ratings (0.5 MW, 1.5 MW, 5 MW). The total harnessed energy in the Ouessant site is calculated for each power rating. According to the optimization results, the gear ratio (3:1) is the optimal one whatever the power level is (Figure 13). When it is less than (5:1), geared systems are cheaper than direct-drive ones. Concerning the estimated TST cost per kWh (Figure 14), the 1.5 MW and 5 MW TST energy is cheaper than the 500 kW TST one. It seems that a rated power around 1.5 MW for the Ouessant site is more preferable than very high power ratings.

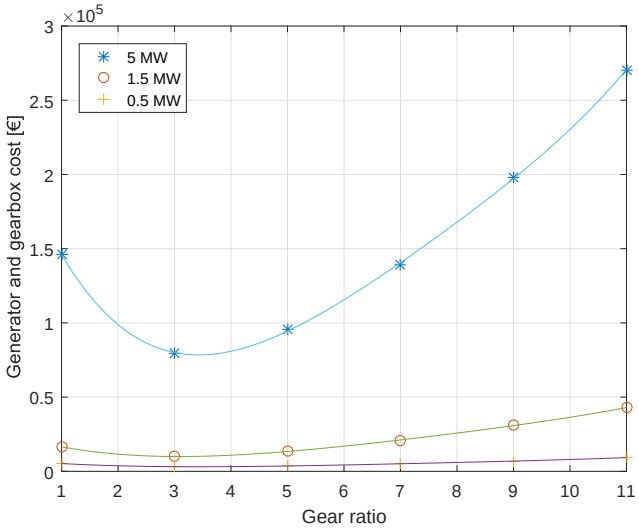

Figure 13. Tidal stream turbine (TST) estimated cost for different gear ratios and different power ratings.

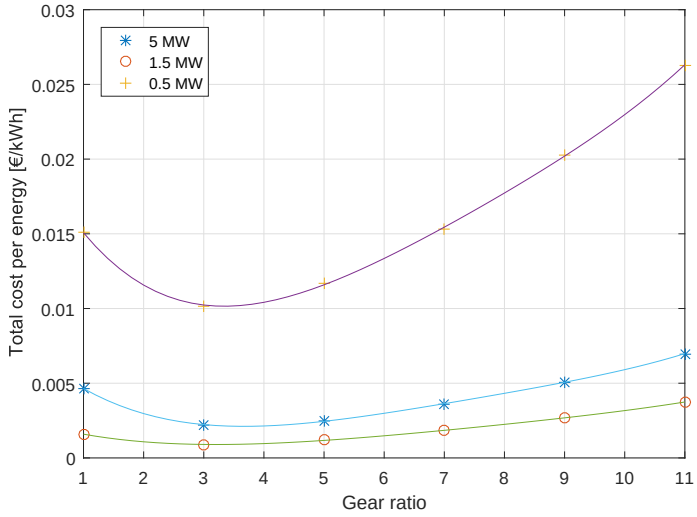

Figure 14. TST total estimated cost per kWh.

As shown in Figure 15, the generator and gearbox cost estimations are separately presented at the power of 1.5 MW. For high gear ratios the gearbox cost increases exponentially while the generator cost decreases slightly. The generator cost is however highly reduced when the gearbox ratio changes from (1:1) (direct-drive) to (3:1). The comparison shows that gearbox low ratios are more interesting especially when the power rating is high but for higher gear ratios the direct-drive configuration is preferable.

The second part considers the 1.5 MW generator's active materials cost and weight. Figure 16 shows that the direct-drive system is the heaviest one compared to the other configurations. On the other hand, the weight of the (3:1) geared generator is around 35% of the total weight of the direct-drive generator.

Regarding PMG active materials cost (Figure 17), the direct-drive configuration is the most expensive and permanent magnet's cost is extremely high compared to the other material's costs. However, the multibrid generator's active materials costs are more balanced especially when the gear ratio is high. In Figure 18 the direct-drive configuration cost is taken as a reference to be compared to

the other configurations cost. As it is shown, the generator's active materials cost is reduced by around 65% when adopting a (3:1) gearbox. For higher gear ratios, cost reduction can reach approximately 85%.

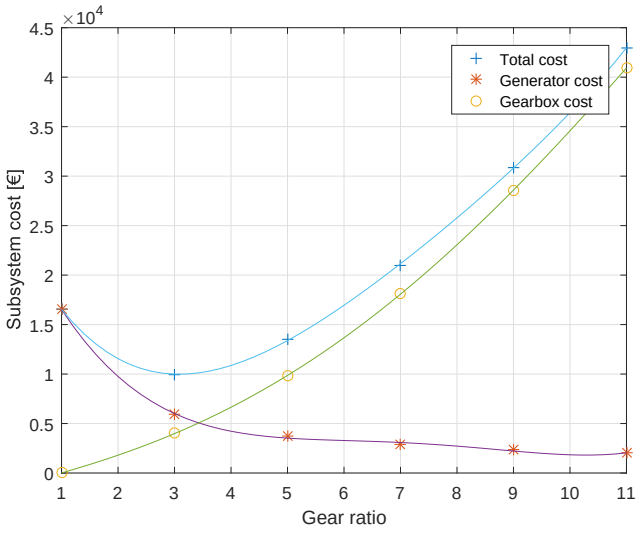

Figure 15. Gearbox and generator costs for different gear ratios at the power rating of 1.5 MW.

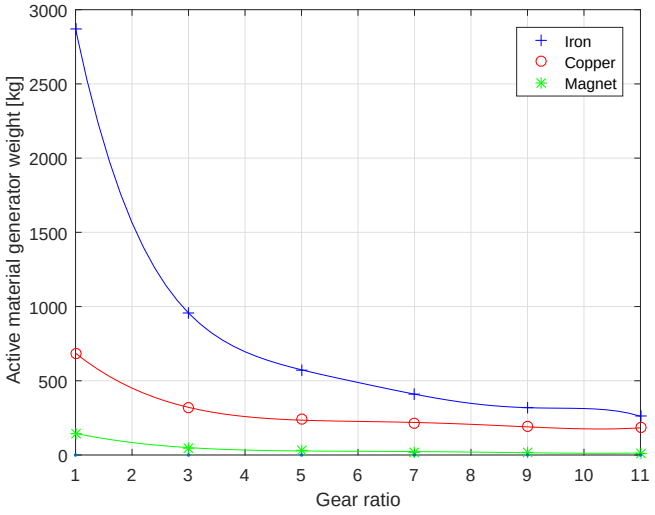

Figure 16. Generator active materials weight for different gear ratios at the power rating of 1.5 MW.

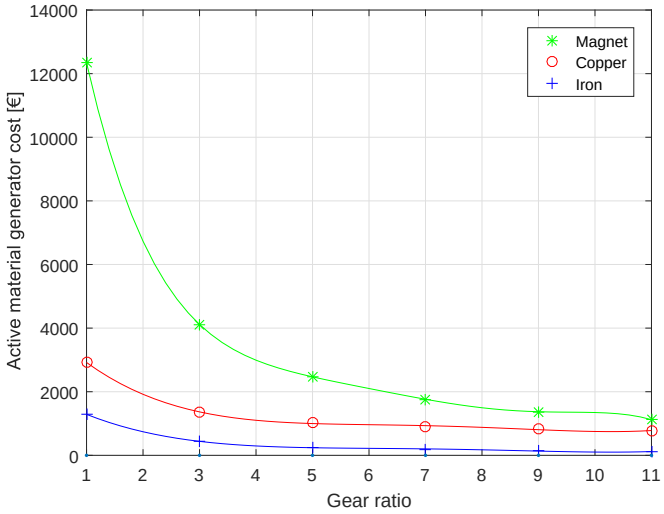

Figure 17. Generator active materials cost for different gear ratios at the power rating of 1.5 MW.

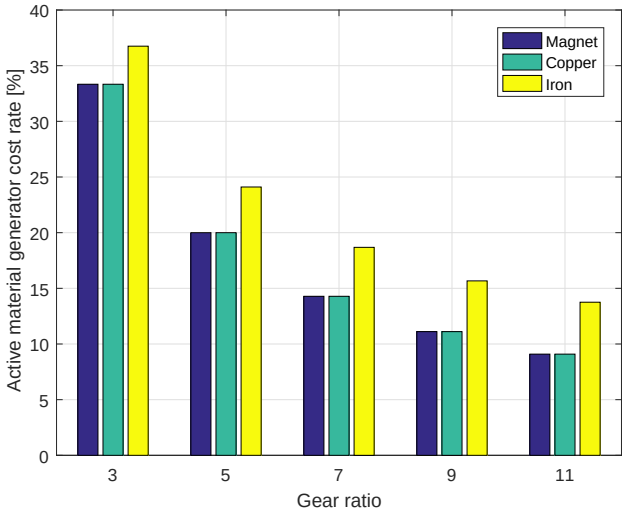

Figure 18. Active material geared generator cost compared to direct drive (DD) generator.

Figure 19 presents four poles of the designed (3:1) geared generator and Figure 20 shows a front and lateral view of the same designed generator at the rating power of 1.5 MW. The two figures give a vision of the designed generator structure and size.

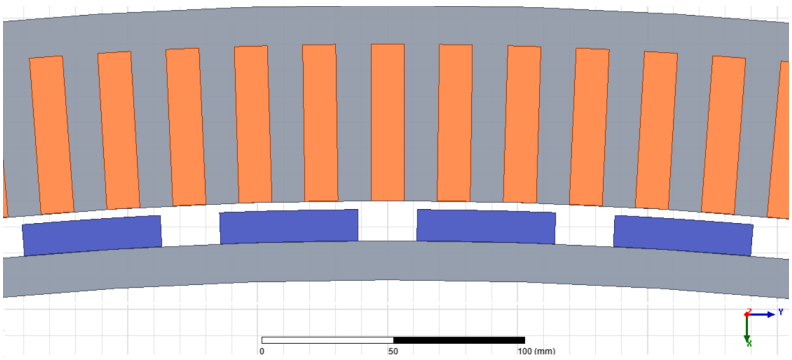

Figure 19. View of the designed (3:1) geared generator at the power rating of 1.5 MW.

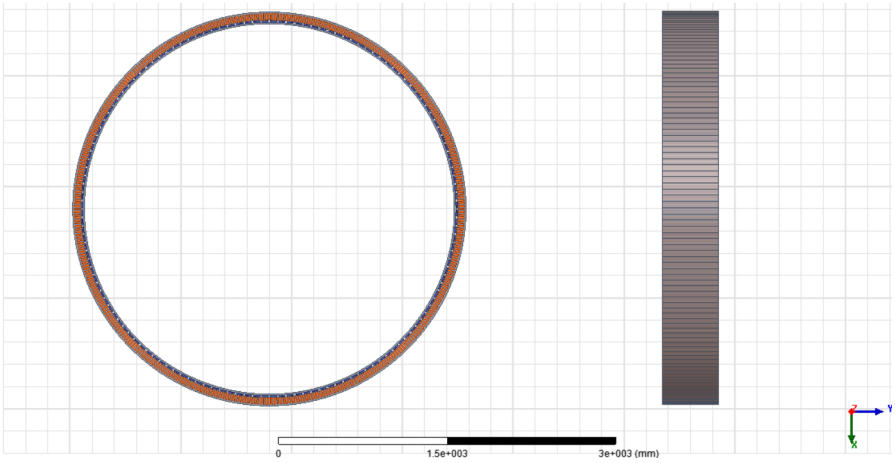

Figure 20. Front and lateral view of the designed (3:1) geared generator at the power rating of 1.5 MW.

From the above-presented results, it is shown that the Multibrid TSTs can be a promising alternative to direct-drive TSTs in terms of weight and cost. According to the Ouessant site energy potential, TSTs power ratings of around 1.5 MW are interesting especially if we consider the limited deepness of the site that limits the turbine diameter. A power rating of 5 MW requires a turbine diameter of 18.8 m, which is interesting if the site allows such a size.

For more accurate estimated cost, the generator structure and manufacturing costs should be considered. Moreover, the TST foundations are not addressed in this study and the gearbox is not deeply designed, which could affect the optimization results. However, these comparative study results could be useful for TST designers and could give them insight on the relevance of the multibrid concept.

5. Conclusions

This paper investigated the application of the multibrid concept for tidal stream turbines. In this context, a design optimization of multibrid permanent magnet generator has been proposed and the system cost-effectiveness has been analyzed by considering the Ouessant site potential energy. A planetary gearbox rough design is proposed for TST systems and the gearbox weight and cost estimations are presented. Furthermore, the study considers a 2D analytical electromagnetic modeling to size the permanent magnet generator. The achieved optimization results clearly showed that multibrid tidal stream turbines are the solution of choice, in terms of weight and cost, when compared to the direct-drive topology. Otherwise, among multibrid systems, lower gear ratios seem preferable, especially for high power ratings. The cost of the 1.5 MW TST is the lowest regarding its harnessed energy in the Ouessent site and it is not far from the 5 MW one. However, a 1.5 MW TST is preferable if the environment constraints are considered where the site deepness is limited.

Author Contributions: Conceptualization, K.T. and M.B.; Methodology, K.T. and M.B.; Software, K.T.; Validation, K.T., M.B., and Z.C.; Formal Analysis, K.T. and M.B.; Investigation, K.T.; Writing–Original Draft Preparation, K.T.; Writing–Review & Editing, K.T., M.B., and Z.C.; Supervision, M.B. All authors have read and agreed to the published version of the manuscript.

Funding: This research received no external funding

Conflicts of Interest: The authors declare no conflict of interest.

Abbreviations

The following abbreviations are used in this manuscript:

TST	Tidal stream turbine
DD	Direct drive
2D	Two-dimensional
PMG	Permanent magnet generator
3D	Three-dimensional
AEP	Annual energy production
PWM	Pulse width modulation

Nomenclature

P_T	Input shaft power
A_t	Turbine blade swept area
ρ	Sea water density
C_p	Power coefficient
λ	Tip speed ratio
λ_{opt}	Optimum tip speed ratio
β	Pitch angle
v_i	Cut-in tidal current speed
v_c	Cut-out tidal current speed
v_n	Rated tidal current speed
P_{Tr}	Rated input shaft power
OCC	Occurrence frequency
FW	Gear face width
d_s	Sun gear diameter
d_p	Planet gear diameter
d_r	Ring gear diameter
K_r	Scaling factor
T_m	Gearbox output shaft torque
K_{ag}	Application factor
K_f	Tooth loads intensity index
W_c	Gearbox weight constant
r_{ratio}	Gearbox ratio
r_{sn}	Gear ratio between sun and planet gears
Z	Planet gears number
c_{gear}	Gearbox specific cost
G_{gear}	Gearbox weight
C_{gear}	Gearbox estimated cost
p_{gear}	Gearbox losses
k_g	Speed-dependent losses constant
P_N	Tidal stream turbine rated power
n_r	Rotor speed
n_{r_N}	Rated rotor speed
T_{EM}	Electromagnetic torque
A_L	Stator current loading
$B_{g_{max}}$	Maximum air-gap flux density
B_g	Air-gap flux density
B_{max}	Saturation flux density
k_{b1}	First harmonic winding factor
ψ	Phase shift between the electromotive force and the current
R_s	Stator radius
L_m	Equivalent core length

ξ_{3D}	3D flow leakage corrective coefficient
k_D	Air-gap coefficient
h_g	Mechanical air-gap
$h_{g'}$	Additional Carter air-gap
k_c	Carter factor
h_m	Magnet height
μ_0	Vacuum permeability constant
μ_{rm}	Magnets relative permeability
B_r	Magnets remanent flux density
$B_{g_{max}}$	Maximum air-gap flow density
τ	Pole pitch
h_{ys}	Stator yoke height
h_{yr}	Rotor yoke height
h_s	Slot height
k_f	Fill factor
β_t	Teeth pitch ratio
p	Pole pairs number
S_{pp}	Slots per pole per phase number
m	Phases number
H_{max}	Maximum magnetic field in the magnet
H_{cj}	Permanent magnet coercive magnetic field
p_{Fe}	Iron losses
f_e	Magnetic field frequency in the iron
p_{Fe0h}	Specific hysteresis loss
p_{Fe0e}	Specific eddy current loss
N_s	Phase winding number of turns
L_{sl}	Leakage inductance
C_{conv}	Power electronics cost
C_g	Permanent magnet generator cost
C_{TST}	Tidal stream turbine cost
c_{Cu}	Copper specific costs
c_{Fe}	Iron specific costs
c_m	Permanent magnet specific costs
G_{Cu}	Copper specific weight
G_{Fe}	Iron specific weight
G_m	Permanent magnet specific weight
$\mathbb{D}$	Set of possible solutions
f_{max}	Maximum electrical frequency

References

1. Benbouzid, M.; Titah-Benbouzid, H.; Zhou, Z. *Ocean Energy Technologies*; Abraham, M.A., Ed.; Encyclopedia of Sustainable Technologies; Elsevier: Amsterdam, The Netherlands, 2017; pp. 73–85, ISBN 978-0-128-04677-7.
2. Selin, N.E. Tidal Power. April 2019. Available online: https://www.britannica.com/science/tidal-power (accessed on 6 June 2019).
3. Flambard, J.; Amirat, Y.; Feld, G.; Benbouzid, M.; Ruiz, N. River and Estuary Current Power Overview. *J. Mar. Sci. Eng.* **2019**, *7*, 365. [CrossRef]
4. Zhou, Z.; Benbouzid, M.; Charpentier, J.F.; Scuiller, F.; Tang, T. Developments in large marine current turbine technologies–A review. *Renew. Sustain. Energy Rev.* **2017**, *71*, 852–858. [CrossRef]
5. Djebarri, S.; Charpentier, J.F.; Scuiller, F.; Benbouzid, M. Comparison of direct-drive PM generators for tidal turbines. In Proceedings of the 2014 International Power Electronics and Application Conference and Exposition, Shanghai, China, 5–8 November 2014; pp. 474–479.

6. Zeinali, R.; Keysan, O. A Rare-Earth Free Magnetically Geared Generator for Direct-Drive Wind Turbines. *Energies* **2019**, *12*, 447. [CrossRef]
7. Keysan, O.; McDonald, A.S.; Mueller, M. A direct drive permanent magnet generator design for a tidal current turbine (SeaGen). In Proceedings of the 2011 IEEE International Electric Machines & Drives Conference (IEMDC), Niagara Falls, ON, Canada, 15–18 May 2011; pp. 224–229.
8. Djebarri, S.; Charpentier, J.F.; Scuiller, F.; Benbouzid, M. Design methodology of permanent magnet generators for fixed-pitch tidal turbines with overspeed power limitation strategy. *J. Ocean. Eng. Sci.* **2019**. [CrossRef]
9. Ozturk, S.; Fthenakis, V.; Faulstich, S. Failure Modes, Effects and Criticality Analysis for Wind Turbines Considering Climatic Regions and Comparing Geared and Direct Drive Wind Turbines. *Energies* **2018**, *11*, 2317.
10. Touimi, K.; Benbouzid, M.; Tavner, P. A Review-based Comparison of Drivetrain Options for Tidal Turbines. In Proceedings of the 2018 IEEE International Power Electronics and Application Conference and Exposition (PEAC), Shenzhen, China, 4–7 November 2018; pp. 1–6.
11. Touimi, K.; Benbouzid, M.; Tavner, P. Tidal stream turbines: With or without a Gearbox? *Ocean. Eng.* **2018**, *170*, 74–88. [CrossRef]
12. Li, H.; Chen, Z.; Polinder, H. Optimization of multibrid permanent-magnet wind generator systems. *IEEE Trans. Energy Convers.* **2009**, *24*, 82–92. [CrossRef]
13. Detailed Technical-Specification WWD-3. Available online: http://www.ecosource-energy.bg/uploads/Technical_Specification_WWD3.pdf (accessed on 6 June 2019).
14. Multibrid M5000. Available online: https://en.wind-turbine-models.com/turbines/22-multibrid-m5000 (accessed on 6 June 2019).
15. Xu, Q.; Li, W.; Lin, Y.; Liu, H.; Gu, Y. Investigation of the performance of a stand-alone horizontal axis tidal current turbine based on in situ experiment. *Ocean. Eng.* **2016**, *113*, 111–120. [CrossRef]
16. Polinder, H.; Van der Pijl, F.F.; De Vilder, G.J.; Tavner, P.J. Comparison of direct-drive and geared generator concepts for wind turbines. *IEEE Trans. Energy Convers.* **2006**, *21*, 725–733. [CrossRef]
17. Hart, K.; McDonald, A.; Polinder, H.; Corr, E.J.; Carroll, J. Improved cost energy comparison of permanent magnet generators for large offshore wind turbines. In Proceedings of the European Wind Energy Association 2014 Annual Conference, Barcelona, Spain, 10–13 March 2014.
18. Djebarri, S.; Charpentier, J.F.; Scuiller, F.; Benbouzid, M. Design and performance analysis of double stator axial flux PM generator for rim driven marine current turbines. *IEEE J. Ocean. Eng.* **2015**, *41*, 50–66.
19. Titah-Benbouzid, H.; Benbouzid, M. Biofouling issue on marine renewable energy converters: A state of the art review on impacts and prevention. *Int. J. Energy Convers.* **2017**, *5*, 67–78. [CrossRef]
20. Mycek, P.; Gaurier, B.; Germain, G.; Pinon, G.; Rivoalen, E. Experimental study of the turbulence intensity effects on marine current turbines behaviour. Part I: One single turbine. *Renew. Energy* **2014**, *66*, 729–746. [CrossRef]
21. SHOM (Service Hydrographique et Ocanographique de la Marine), 3D Marine Tidal Currents in Fromveur (Ouessant island). 2014. Available online: https://diffusion.shom.fr/pro (accessed on 6 June 2019).
22. El Tawil, T.; Charpentier, J.F.; Benbouzid, M. Tidal energy site characterization for marine turbine optimal installation: Case of the Ouessant Island in France. *Int. J. Mar. Energy* **2017**, *18*, 57–64. [CrossRef]
23. Radzevich, S.P. *Dudley's Handbook of Practical Gear Design and Manufacture*; CRC Press: Boca Raton, FL, USA, 2012.
24. Guo, Y.; Parsons, T.; King, R.; Dykes, K.; Veers, P. *Analytical Formulation for Sizing and Estimating the Dimensions and Weight of Wind Turbine Hub and Drivetrain Components*; Technical Report; National Renewable Energy Lab. (NREL): Golden, CO, USA, 2015.
25. Harrison, R.; Hau, E.; Snel, H. *Large Wind Turbines: Design and Economics*; Wiley: Chichester, UK, 2000; Volume 1.
26. Rourke, F.O.; Boyle, F.; Reynolds, A. Marine current energy devices: Current status and possible future applications in Ireland. *Renew. Sustain. Energy Rev.* **2010**, *14*, 1026–1036. [CrossRef]
27. Dubois, M.R. Review of electromechanical conversion in wind turbines. *Rep. EPP00* **2000**, *3*, 4–10.
28. Djebarri, S. Contribution à la Modelisation et à la Conception Optimale de Generatrices à Aimants Permanents Pour Hydroliennes. Ph.D. Thesis, Université de Bretagne Occidentale, Brest, France, 2015.

29. Djebarri, S.; Charpentier, J.F.; Scuiller, F.; Benbouzid, M.; Guemard, S. Rough design of a double-stator axial flux permanent magnet generator for a rim-driven marine current turbine. In Proceedings of the 2012 IEEE International Symposium on Industrial Electronics, Hangzhou, China, 28–31 May 2012; pp. 1450–1455.
30. Pyrhonen, J.; Jokinen, T.; Hrabovcova, V. *Design of Rotating Electrical Machines*; John Wiley & Sons: Chichester, UK, 2013.
31. Böhmeke, G. Development and Operational Experience of the Wind Energy Converter WWD-1. In Proceedings of the 2003 Europ Wind Energy Conference, Madrid, Spain, 16–19 June 2003.
32. Boldea, I. *The Electric Generators Handbook-2 Volume Set*; CRC Press: Boca Raton, FL, USA, 2005.
33. Grauers, A. Efficiency of three wind energy generator systems. *IEEE Trans. Energy Convers.* **1996**, *11*, 650–657. [CrossRef]
34. Xue, Y.S.; Han, L.; Li, H.; Xie, L.D. Optimal design and comparison of different PM synchronous generator systems for wind turbines. In Proceedings of the 2008 International Conference on Electrical Machines and Systems, Wuhan, China, 17–20 October 2008; pp. 2448–2453.